

# **Acoustic Intra-Body Data Transmission**

*Innervation, Inc. (Columbia, Maryland, USA):*

**Yuri Okunev, Michael Arneson, William Bandy,  
Roger Davenport, Brian Jamieson, Kevin Powell, Wayne Shanks, Angelo Trivelli**

## **ABSTRACT**

Data transmission is one of the most important procedures of the capsule endoscopy technology, which provides patients and physicians with a non-invasive method for diagnosing GI disorders in the small bowel. Data transmission from the capsule to an external data recording system is usually accomplished with an RF data communications channel. It is proposed here to use ultrasound waves for transmission of images and telemetry information from a capsule inside a human body to outside receivers – the acoustic intra-body data transmission system. A physical model of the intra-body acoustic channel is presented, and architecture, schemes and signal processing algorithms of acoustic transmitters and receivers are considered. Digital and analog modulation/demodulation (modem) schemes for multi-path and single-path acoustic channels are proposed. Results of stochastic simulation and experimental testing of the proposed acoustic systems are discussed.

## **Introduction**

There is a large and growing worldwide market for capsule endoscopy [1]. Just within the United States it is estimated that there are 95 million cases of GI disorders per year that result in 30 million office visits and 15 million diagnostic therapeutic procedures per year. Capsule endoscopy will support the growing need of diagnostic procedures, providing the patient with a non-invasive alternative and physicians with an additional method for diagnosing GI disorders. The commercial validity of capsule endoscopy has already been demonstrated by the first generation of products [2].

Transmission of images and telemetry information from a capsule inside a human body to outside receivers is one of the most important procedures of the capsule endoscopy technology. Existing intra-body data transmission technology is based on electro-magnetic radiation – radio frequency (RF) systems [3], or on electro-static propagation – galvanic systems [4].

Innervation's data transmission system is the first and only capsule endoscopy system that uses an acoustic communication protocol for data transfer. Innervation's capsule endoscopy system consists of three main components: a pill, a receiver, and a workstation. The pill is a small, battery operated, swallowable capsule that contains scanning technology to collect images throughout the gastrointestinal tract. The images are transmitted to the receiver through an acoustic channel and then uploaded to the workstation where the physician can then view the images. Acoustic signaling, versus RF signaling, enables ultra low power data transmission, of a magnitude of about 1000 times less energy than RF. This power efficiency allows for a very small battery and, therefore, a smaller pill size. Additionally, acoustic transmission will allow physicians to determine the exact location of the pill in the GI tract when a problem area is detected, a feature not available with current RF products.

It should be noted that ultrasound waves were successfully used for telemetry data transmission in underwater acoustic systems many decades [5]. As a rule, the underwater acoustic systems provide comparatively low data rate transmission at considerable power radiation. In contrast,

transmission of images and telemetry information from a capsule inside a human body to outside receivers requires comparatively high data rate with severe restrictions on radiated power, energy and computation resources.

This paper is organized as follows.

Section 1 contains brief description of a physical model and main parameters of the intra-body acoustic channel.

Section 2 describes transceivers and modems for multi-path intra-body acoustic channels based on, first, frequency hopped signals with combined frequency-phase modulation and, second, multi-frequency signals with differential phase modulation of sub-carriers.

Section 3 describes transceivers and modems for single-path intra-body acoustic channels based on digital and analog modulation schemes: digital single-carrier system with differential quadrature phase shift keying, digital multi-receiver system with quadrature accumulation of partial signals, and analog systems with single side-band modulation and double side-band modulation.

## 1. Physical model of the intra-body acoustic channel.

Attenuation of ultrasound waves in the body depends considerably on both carrier frequency and propagation distance. According to results obtained in our laboratory, average attenuation  $A$  dB of the ultrasound signal inside the human body can be approximated as follows:

$$A \approx 0.75LF \text{ dB}, \quad (1)$$

where  $L$  cm – distance between a capsule transmitter inside a human body and an external receiver on the surface of the human body, and  $F$  MHz – carrier frequency.

Another important phenomenon of the intra-body acoustic channel is severe multi-path propagation, caused by reflections of acoustic waves from different objects (tissues) inside the body, surface areas, surface boundaries, and interfaces in the channel environment. Superposition of the main shortest-path ray and numerous echo rays causes both inter-symbol interference and signal fading at the receiver. However, both of these effects weaker at increased carrier frequency. Let us consider two propagation paths (rays) from the transmitter to the receiver with path distances  $L_1$  and  $L_2$ , where  $L_2 > L_1$ . Attenuations of these rays are equal to  $A_1 = 0.75L_1F$  dB and  $A_2 = 0.75L_2F$  dB, correspondingly. If the first ray can be considered as the useful signal, and the second ray – as the interference, then the signal-to-interference ratio (SIR) at the input of the receiver is equal to

$$\text{SIR} = -A_1 + A_2 = 0.75(L_2 - L_1)F \text{ dB}. \quad (2)$$

Expression (2) shows that SIR at the input of the receiver in the multipath intra-body acoustic channel depends considerably on the carrier frequency. In other words, with increasing the acoustic carrier frequency the influence of delayed rays decreases. For example, at  $F=1$  MHz and  $(L_2 - L_1)=10$  cm, the  $\text{SIR}=7.5$  dB, but at  $F=2$  MHz and the same distance  $(L_2 - L_1)=10$  cm, the  $\text{SIR}=15$  dB. Simulation of multipath signal processing shows that at a bit error rate (BER) of 0.001, the influence of any delayed ray can be neglected if it is less than the main ray by at least 12 dB. Using this assumption and based on formula (2), we can conclude that at  $F=2$  MHz any acoustic ray with delay more than 8 cm relatively the main ray can be neglected.

The above consideration shows that the ultrasound intra-body channel can be conditionally divided into three main frequency areas: the multi-path area with the carrier

frequency below 1.0 MHz, the single-path area with the carrier frequency above 2.0 MHz, and the transient area between 1.0 MHz and 2.0 MHz with progressive transition from the multi-path channel to the single-path channel.

In the multi-path frequency area, a structure of the intra-body acoustic channel is dynamically changed in time, namely, a number of considerable rays, their attenuations and delays are random functions of time. These variations in the channel are caused both by motion of the capsule-transmitter inside the body and by changes in the non-static environment (tissues and liquid movement around the capsule-transmitter). So, the physical model of the multi-path intra-body acoustic channel may be briefly described as follows:

- the signal at the input of the receiver is a sum (superposition) of a random number of transmitted signals (rays) subjected to linear transforms;
- each component of the sum has random delay relatively the other components, and this delay is within some fixed time interval  $\Delta\tau$ ;
- each component of the sum is randomly attenuated (faded) with the average attenuation depending on its delay.

Some parameters of this model can be estimated based on the corresponding experimental and theoretical results.

Maximum path delay  $\Delta\tau$ , which is called the multipath interval, is an important system parameter because it determines the interval of inter-symbol interference. The multipath interval can be estimated from the above assumption that the influence of any delayed ray can be neglected if it is less than the main ray by 12 dB. For example, at carrier frequency  $F=1$  MHz, maximum distance between two essential ultrasound rays according to (2) is equal to  $\Delta\tau = \max(L_2 - L_1) = 12/0.75 = 16$  cm. At ultrasound speed 1500 m/s, it corresponds to  $\Delta\tau = 16/1500 = 10.7 \mu\text{s}$ . This result is well matching with the experiment, which has shown duration of visible channel pulse response about 150  $\mu\text{s}$  at the acoustic carrier near 1 MHz.

Stochastic distribution of the ray attenuation is conventionally described by Rayleigh, Ricean, Nakagami, or Lognormal rules [6]. There are some similarities between fading in the intra-body acoustic channel and in the underwater acoustic channel [7], but there are also considerable differences caused by strongly restricted area of ultrasound propagation inside the body. Therefore it is reasonable to assume that there is considerable similarity between fading in intra-body acoustic channels and fading in indoor radio channels. Comprehensive experimental studies of the indoor wireless channels have shown that the Log normal distribution is the best mathematical model for indoor fading [8].

**Fig. 1 Distribution of the delayed ray**

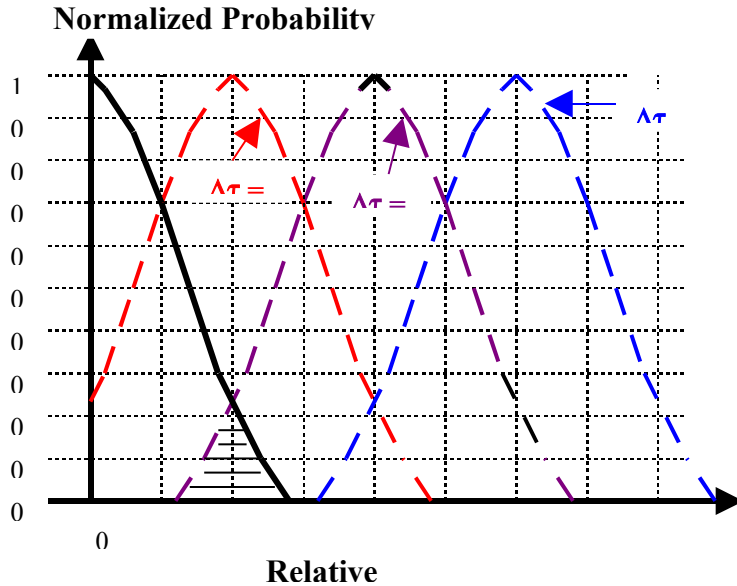


Fig. 1 illustrates the Lognormal distribution of signal attenuation for several equiprobable rays with different delays in the ultrasound intra-body channel at 1 MHz carrier frequency and standard deviation of attenuation  $\sigma=5$ . Coordinate Y in this chart is the normalized probability density of the ray attenuation relatively the ray with the minimum delay:  $P(A) \cdot (5\sqrt{2\pi})$ . Coordinate X in this chart is the ray attenuation A dB. There are 4 plots in Fig. 1, corresponding (from left to right) to a ray with minimum absolute delay, a ray with 45 us delay relative to the ray with minimum absolute delay, a ray with 90 us delay, and a ray with 140 us delay. Average attenuation for each ray is calculated according to (1). It should be noted that probability densities of signals with different delays are overlapped in Fig.1. This means that according to the considered model, the amplitude of a signal with larger delay may be larger than the amplitude of a signal with less delay, exactly as it has been considered in the lab experiments. For example, the amplitude of the signal with 90 us delay may be larger than the amplitude of the signal with minimum absolute delay. Probability of this event is equal to the area of the shaded triangle around the 5 dB point: in this area attenuation of the signal with minimum absolute delay is more than 5 dB, and attenuation of the signal with 90 us delay is less than 5 dB.

Considerable differences in ultrasound signal processing in comparison with radio signals processing are caused by the delay phenomenon of the acoustic channel. The delay difference between ultrasound signals in two outside receiver is much more considerable than in the case of radio receivers. For example, if the distance difference between the capsule and two receivers is equal to 15 cm, then the relative delay for electromagnetic signals will be negligible, namely,  $5E-7$  us; however, at the same example, the relative delay for ultrasound signals will be equal to 100 us. This phenomenon in its turn causes at least three important consequences.

First, in contrast to RF signals, the acoustic signal delays become measurable even for small distances – it allows the intra-body acoustic system to provide location of the capsule by means of measuring relative signal delays between several external receivers.

Second, in contrast to RF systems, even several millimeters of separation between receivers in the 1-2 MHz frequency range is enough for providing efficient mitigation of space selective fading. Indeed, efficient space diversity in fading channels conventionally requires about one wave length separation of the receiving antennas; in RF systems with 1 MHz carrier the wave length is equal to 300 m, but in acoustic system with 1 MHz carrier the wave length is equal to 1.5 mm.

Third, in contrast to RF systems, optimal multi-receiver processing of the ultrasound signals, based on accumulation of partial signals, requires signal delay equalization in the multi-receiver processor.

The above peculiarities of the intra-body acoustic channel will be additionally discussed below at specific modulation schemes consideration.

## **2. Modems for multi-path intra-body acoustic channels**

There are several approaches to development of encoding/modulation schemes for data transmission in multi-path channels [9]. FH (Frequency Hopping) and OFDM (orthogonal frequency division multiplexing) technologies are the most promising approaches to high data rate transmission in the multi-path intra-body acoustic channels. However, conventional FH and OFDM modulation schemes need some improvement and modification to meet adequately specific technical requirements and restrictions of those channels.

### **2.1. FH-FSSK-DPSK system: Frequency Hopped (FH) signal with combined Frequency Set Shift Keying (FSSK) and Differential Phase Shift Keying (DPSK)**

FH-FSSK-DPSK data transmission is based on a FH carrier with primary frequency modulation. Frequency hopping allows the system to avoid inter-symbol interference in the multi-path acoustic channel, if a FH cycle exceeds multi-path interval. The FH carrier consists of a sequence of pulses with different frequencies from  $K$  sets of frequencies. Utilization of a current transmitted pulse from one of  $K$  sets of frequencies allows the system to provide transmission of  $\log K$  bits per a FH pulse – this type of modulation we call frequency set shift keying (FSSK).

Let us illustrate the method based on the simplest binary FSSK modulation utilizing two sets of FH carriers. The first set  $\{f\}$  contains  $N$  carriers:  $f = \{f_1, f_2, \dots, f_N\}$ , and the second set  $\{F\}$  also contains  $N$  carriers:  $F = \{F_1, F_2, \dots, F_N\}$ . Within the FH cycle, containing  $N$  time slots, carriers from both sets are transmitted sequentially, namely: in the  $i$ -th slot of the FH cycle the transmitter transmits either  $f_i$  or  $F_i$  carrier depending on the current data symbol, and, correspondingly, the receiver expects either  $f_i$  or  $F_i$  carrier. The receiver should detect which carrier  $f_i$  or  $F_i$  is more likely in the  $i$ -th slot, and make corresponding decision in favor of data “0” or “1”.

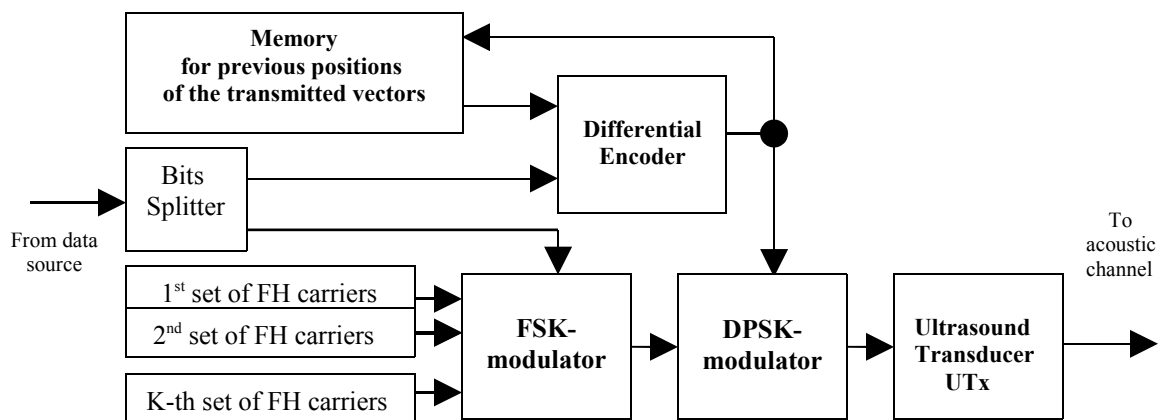
The best detection results are achieved when all FH pulses are orthogonal waveforms. For example, if a pulse duration is  $\Delta t = 20$   $\mu$ s, then the orthogonal frequency interval within both frequency sets is  $\Delta f = \Delta F = 50$  kHz. On the other hand, if the multi-path interval is  $\Delta \tau = 100$   $\mu$ s, then each FH cycle should contain at least 5 pulses with duration  $\Delta t = 20$   $\mu$ s. As the result, each set of frequencies takes total bandwidth about 250 kHz. In this scenario, each set of frequencies can be radiated by a separate acoustic transducer. Non-orthogonal sets of frequencies take a lesser total bandwidth, but they do not provide maximum noise immunity.

Additional phase modulation can be used with the FH-FSSK acoustic modulation scheme in order to increase data rate. Methods of additional phase modulation are based on either changing a phase difference between FH pulses with the same frequency or changing a phase difference within each FH pulse.

The algorithm of DPSK modulation by changing phase difference between FH pulses can be described as follows: if in the  $i$ -th slot of the FH cycle the transmitter transmits a pulse with frequency  $f_i$  from set  $\{f\}$ , then its phase is properly shifted relatively the phase of the latest previous pulse with the same frequency  $f_i$ ; and, on the contrary, if in the  $i$ -th slot of the FH cycle the transmitter transmits a pulse with frequency  $F_i$  from set  $\{F\}$ , then its phase is properly shifted relatively the phase of the latest previous pulse with frequency  $F_i$ . The above phase shift (phase difference) depends on both transmitted data and the number of phase difference positions utilized; for example, at the DQPSK modulation the phase shifts may be  $0, \pi/2, \pi,$  or  $3\pi/2$  radian.

**Fig.2 Block-diagram of the FH-FSSK acoustic system with additional DPSK modulation by changing a phase difference between FH pulses**

**a) Transmitter**



**b) Receiver**

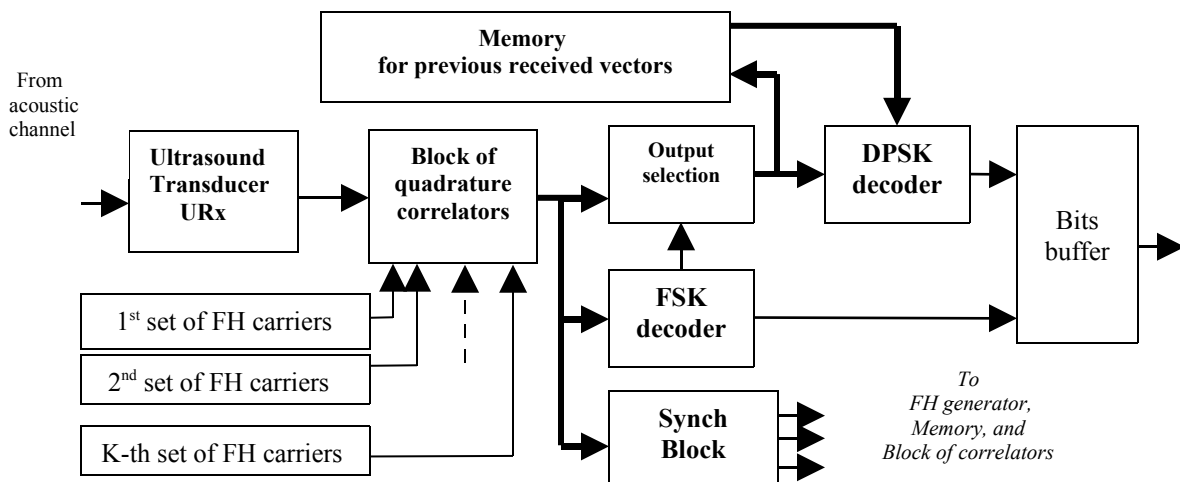


Fig. 2 shows a block-diagram of the acoustic system with FH-FSSK-DPSK modulation.

In the transmitter (Fig.2a), the input bit stream is first split into bits for FSSK modulation and bits for DPSK modulation. The  $\log_2 K$  bits for FSSK are directly fed to an FSK-modulator, which selects the carrier from one of  $K$  sets of FH carriers, generated by the FH carrier generator. The  $\log_2 M$  bits for DPSK are fed to a differential encoder, which are connected to memory. The function of the memory unit is to provide the differential encoder with the previous position of transmitted vectors for all FH carriers, and, at the same time, to save the current position of transmitted vectors for all FH carriers. The number of cells in the Memory depends on both the number of FH sets  $K$  and the number of sub-carriers in each set  $N$ . Generally, the number of cells in the Memory is equal to  $KN$ , and each cell should save  $M$ -ary number, where  $M$  is a number of phase positions. The differential encoder outputs signal for a DPSK modulator, which shifts properly the phase of the current carrier, previously selected by the FSSK modulator. Finally, the FSSK-DPSK modulated carrier stimulates the ultrasound transducer, which radiates the signal to the acoustic channel.

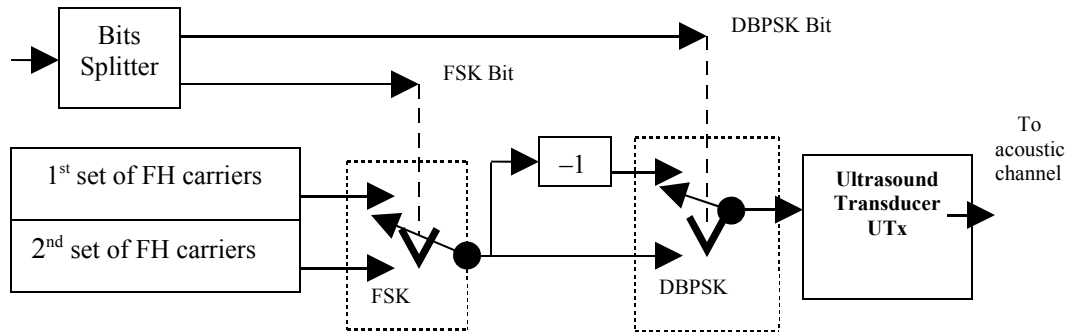
In the receiver (Fig.2b), the received signal from the output of the URx is fed to the block of quadrature correlators. A FH-carrier generator outputs  $K$  carriers in parallel during each pulse interval – these carrier are used as reference signals in the quadrature correlators. Correlation coefficients, calculated in the block of quadrature correlators, i.e.  $2K$  quadrature projections of the received signal on  $K$  reference signals, are fed to the FSK decoder. The last one makes decision in favor of the most likely carrier and provides  $\log K$  bits to the bits buffer. The FSK decision is also used in the selection unit for selection a pair of correlation coefficients (current projections of the received signal), corresponding to the most likely carrier. The selected pair of correlation coefficients is saved the memory for the previously received vectors. Then the DPSK decoder makes a decision in favor of the most likely phase difference by comparing the received projections with previous projections of the same carrier saved in the memory, and provides the bits buffer with additional  $\log M$  bits. It should be noted that synchronous operation of the FH generator, the quadrature correlators, and the memory is supported by the synchronization block, providing FH pulse and symbol timing.

Data rate in the system in Fig.2 depends on number  $K$  of FH sets and number  $M$  of phase positions, and it is equal to  $[(\log_2 K + \log_2 M)/T]$  bit/s, where  $T$  is the pulse duration. For example, at FH pulses with 20  $\mu$ s duration,  $K=2$ , and  $M=4$  (DQPSK) the system provides data rate 150 kbit/s.

Another method of additional phase modulation of the FH-FSSK acoustic signal can be realized by a phase shift within each FH time slot. This means that each FH pulse is divided into two parts with phase difference between these two parts corresponding to the transmitted data. For example, at binary DPSK modulation (DBPSK), the  $0^\circ$  phase-shift for data-0 and  $180^\circ$  phase-shift for data-1 are used. At 4-ary DPSK modulation (DQPSK), the phase-shifts are:  $0^\circ$  phase-shift for data-00,  $90^\circ$  for data-01,  $180^\circ$  for data-11, and  $270^\circ$  for data-10. The receiver should detect the most likely phase-shift within each FH time slot and make decision in favor of the corresponding bit or bit combination. It should be noted that this method of FH-FSSK-DPSK modulation is easier than the previous one, because the phase shift is carried out inside each pulse – the method does not need to save the previous phase position for all frequencies, however, it requires double bandwidth because of phase changing inside the pulse.

**Fig.3 Block-diagram of the FH-FSSK acoustic system with DBPSK modulation by changing a phase difference inside FH pulses**

**a) Transmitter**



**b) Receiver**

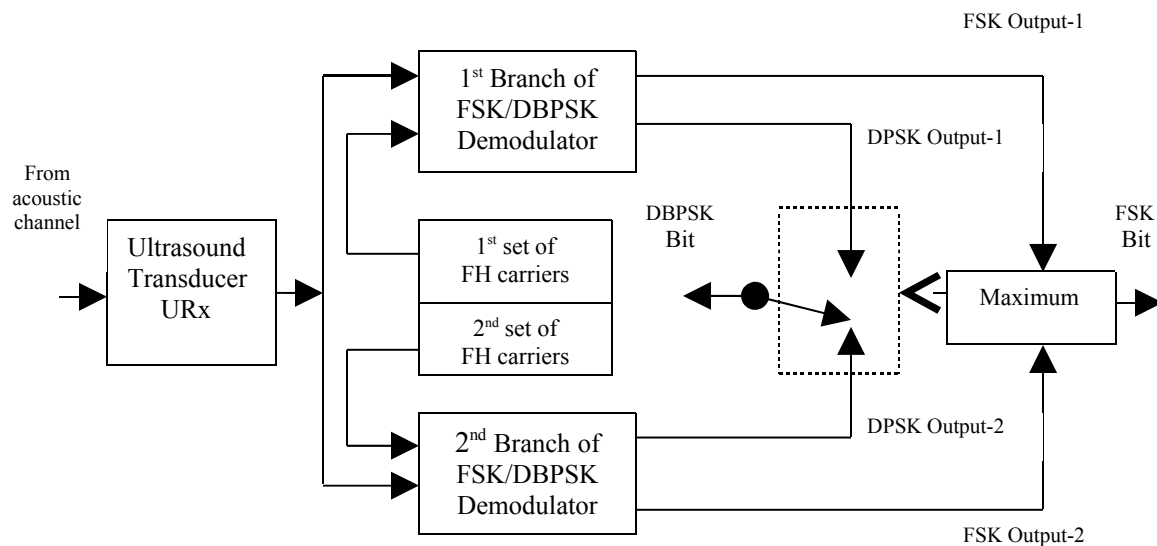


Fig.3 shows a block-diagram of the simplest ultrasound system with 2-set FH-FSSK modulation and with additional binary DBPSK modulation by  $180^\circ$  phase changing inside the FH pulse.

In the transmitter (Fig.3a), the input bit stream is split into two bit streams: FSK bits and DBPSK bits. The FSK bit controls the FSK modulator comprising a two-position switch; the switch outputs one of two carriers from the FH carrier generator depending on the current FSK bit. The DBPSK bit controls the DBPSK modulator comprising a two-position switch, identical to the FSK modulator; the switch outputs the direct or inverse carrier from the output of the FSK modulator depending on the DBPSK bit. It should be noted that DBPSK switching moment is shifted by a half of bit interval relatively FSK switching moment. Synchronization of FH generator, FSK and DBPSK modulators is provided by bit timing.

In the receiver (Fig.3b), the received signal is in parallel fed to the 1<sup>st</sup> and 2<sup>nd</sup> branches of the combined FSSK/DBPSK demodulator. The branches are absolutely identical, but the 1<sup>st</sup> branch uses the reference signal from the generator of the 1<sup>st</sup> set of FH carriers  $\{f\}$ , and the 2<sup>nd</sup> branch uses the reference signal from the generator of the 2<sup>nd</sup> set of FH carriers  $\{F\}$ . The generators synchronously generate a pairs of FH carriers:  $f_1$  and  $F_1$ ,  $f_2$  and  $F_2, \dots, f_N$  and  $F_N$ . Each branch of the demodulator has two outputs: DBPSK output, containing DBPSK bit decision, and FSK output, containing a signal for FSK bit decision. Two FSK output signals are fed to the FSK decision unit, including maximum estimator. The unit estimates the most likely FH carrier ( $f_i$  or  $F_i$ ) by choosing the maximum among the FSK outputs. This FSK binary decision controls the DBPSK switch, which chooses DBPSK decisions from two DBPSK output signals. It should be noted that the FH generator and the combined FSSK/DBPSK demodulator work synchronously within the symbol interval, which should coincide with the corresponding FH slot.

**Fig. 4 Scheme of the combined FSK/DBPSK demodulator for the receiver in Fig.3b.**

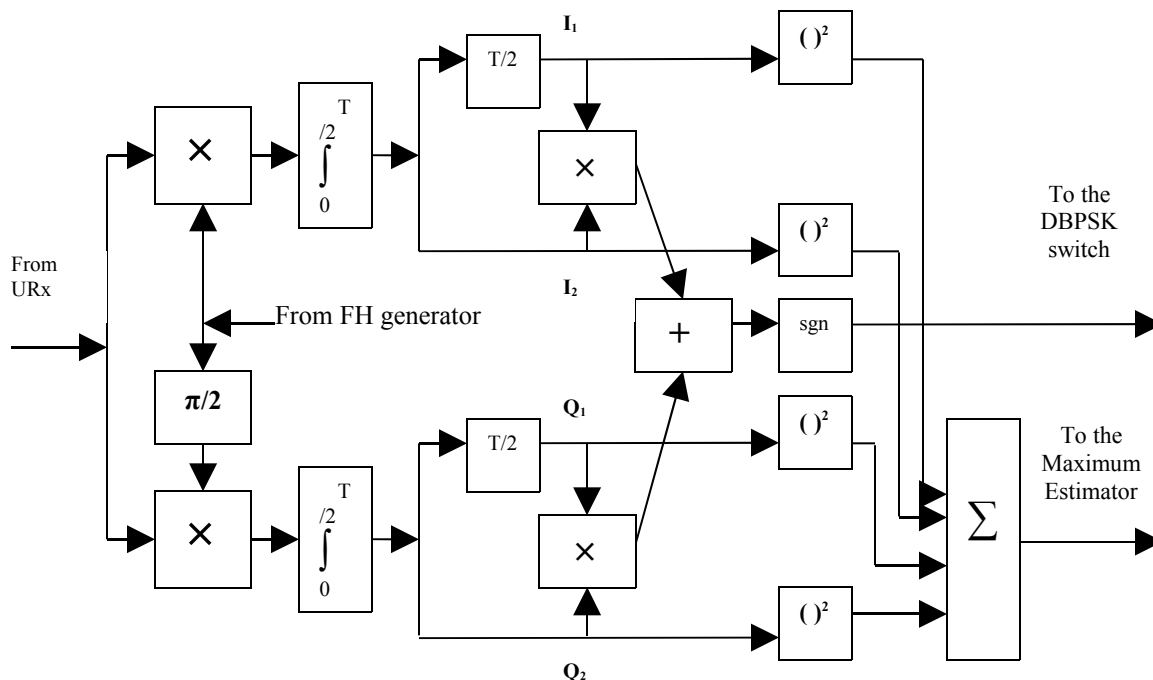


Fig.4 shows a scheme of the combined FSSK/DBPSK demodulator in Fig.3b. The front end of the demodulator is the conventional I/Q correlator (matching filter). The integrator provides signal accumulation within each half-symbol interval  $T/2$ . As a result, after  $T/2$  delay there are 4 signals at correlator outputs:  $I_1$ ,  $I_2$ ,  $Q_1$ , and  $Q_2$ . The further algorithm of decision making for FSK bit  $B_F$  and DBPSK bit  $B_P$  may be described as follows: signal  $S_F = (I_1)^2 + (Q_1)^2 + (I_2)^2 + (Q_2)^2$  is fed to the maximum estimator in scheme Fig.3b, and signal  $B_P = \text{sign}(I_1 I_2 + Q_1 Q_2)$  is fed to the DPSK switch in general scheme Fig.3b.

Stochastic MatLab simulation of the acoustic system with the combined FH-FSSK-DQPSK modulation according to block-diagram Fig.2 has been provided with a model of the AWGN channel. The FH signal included two sets of orthogonal carriers with binary FSK and additional 4-position DQPSK based on Gray encoding (total data rate is equal to 3 bit per the PH pulse). The block of quadrature correlators in the receiver Fig.2b realized the optimal non-coherent processing of both FSK and DQPSK signals. The simulation shows that in order to provide the bit error rate  $BER=0.001$ , the system requires signal-to-noise ratio (in terms of the symbol energy to the noise power spectral density)  $SNR=12.2$  dB at the input of the receiver. It is only 1.2 dB more than the classical binary FSK system needs for transmission of 1 bit per symbol at the optimal non-coherent signal processing.

The FH-FSSK modulation scheme was also implemented experimentally. The system utilized custom acoustic transducers in frequency range 1-2 MHz, and a water tank media, imitating property of the intra-body acoustic channel. Transmit and receive software was implemented on a National Instruments Lab-View platform.

In addition, the FH-FSSK ultrasound modulation scheme was tested to validate the acoustic communication channel for transmission through inside tissue and organs of a pig body. The pig in this measurement was euthanized the same morning as the measurements were taken to ensure the tissue and organs had the same consistency and acoustic properties as a living animal. The high level transmission system consisted of an acoustic transmitter inside of the pig's abdominal cavity, and an acoustic receiver patch outside of the pig's body contacting the pig's skin. The receiver was a custom design PCB board with an Innurvation transducer designed which was fabricated in the Innurvation Laboratory. The patch was connected with a 50 ohm coax cable to the Lab-View platform. The FH-FSSK ultrasound modulation scheme used 2 sets of sub-carriers in frequency range about 1.5 MHz with 4 sub-carriers in each set separated by 20 KHz. The experimental system provided 100 kbit/s data rate.

The test consisted of disassembling a bitmap image and then transmitting it through the acoustic channel with the FH-FSSK and then reassembling the image after signal reception. The image that was used was a pig intestine that was previously captured using a flat plane linear scanner. Lab-View did both the transmit modulation and the receive demodulation and tracked bit errors by comparing transmit bits to received bits. A sequence of the same image was sent through the channel keeping all parameters the same and only varying the transmitter peak to peak voltage signal and then recording the associated BER.

The animal test confirmed that data transmission with BER performance about 0.001 provides high quality image transmission, and that this performance may be achieved at radiated power about 0.1 mWatt. The test also showed that intestinal gas pockets and multiple tissue types did not hinder excellent performance of the acoustic data transmission system.

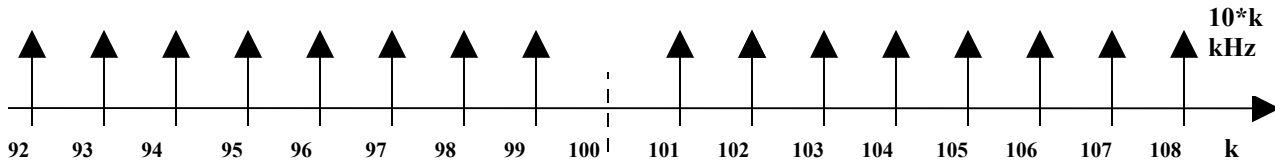
## 2.2. OFDM-DQPSK system: Orthogonal Frequency Division Multiplexing signal with Differential Quadrature Phase Shift Keying modulation of sub-carriers

This system uses multicarrier signal with orthogonal sub-carriers (OFDM signal) and DQPSK modulation of the sub-carriers [10], which can be presented within the symbol interval as follows:

$$S(t) = \sum_{k=K_1}^{K_2} A_k \sin[(k2\pi/T_a)t + \Phi_k], \quad (1)$$

where  $A_k$  and  $\Phi_k$  are the amplitude and phase of the  $k$ -th harmonic (sub-carrier) of the base oscillation with frequency  $\omega_0=2\pi/T_a$ ,  $T_a$  is an interval of sub-carrier orthogonality (active interval).

### a) Frequency Domain



### b) Time Domain

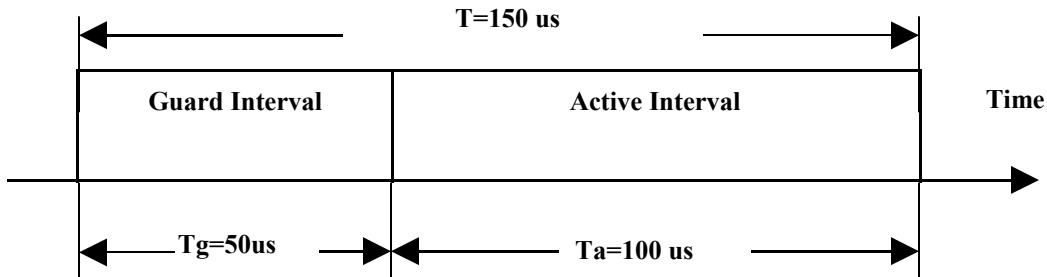


Fig.5 exemplifies a 16 sub-carriers OFDM ultrasound signal in frequency and time domains. The signal contains 16 harmonics of the 10 kHz oscillation. The harmonic numbers from  $K_1=92$  to  $K_2=108$  are indicated under the frequency axis; they correspond to frequencies from 920 kHz to 1080 kHz. The 100<sup>th</sup> harmonic, located exactly in the middle of the spectrum, is not transmitted – this frequency location is used for symbol synchronization. In the time domain, the OFDM symbol with duration  $T$  consists of two parts: a guard interval with duration  $T_g$  and an active interval with duration  $T_a$ . An initial phase of each sub-carrier, bearing information, is changed at the very beginning of the OFDM symbol, i.e. at the beginning of the guard interval, but the receiver provides signal processing only during the active interval. In this example of the acoustic system, the intervals are equal to  $T_g=50 \mu s$ ,  $T_a=100 \mu s$ , and  $T=150 \mu s$ . At these parameters the symbol rate is equal to 6.67 ksymbol/s. If a number of sub-carriers is equal to 16 and the DQPSK modulation is used, the total bit rate will be 213 kbit/s.

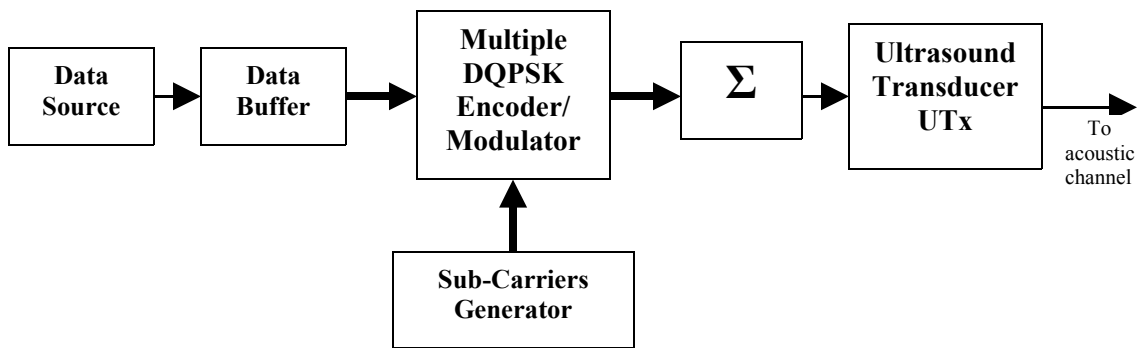
Table 1 illustrates possible parameters of the acoustic OFDM-DQPSK modulation scheme using 16 sub-carriers.

**Table 1. Parameters of the acoustic OFDM-DQPSK scheme using 16 sub-carriers.**

<b>T<sub>a</sub></b> <b>us</b>	<b>T<sub>g</sub></b> <b>us</b>	<b>Sub-carrier Separation kHz</b>	<b>Bit Rate kbit/s</b>	<b>Frequency Efficiency kbit/s/Hz</b>
100	100	10	<b>160</b>	1.0
100	50	10	<b>213</b>	1.3
100	25	10	<b>256</b>	1.6
75	75	13.3	<b>213</b>	1.0
75	50	13.3	<b>256</b>	1.2
75	25	13.3	<b>320</b>	1.5
50	50	20	<b>320</b>	1.0
50	25	20	<b>427</b>	1.3
50	14	20	<b>500</b>	1.6

**Fig. 6 Block-diagram of the OFDM-DQPSK acoustic system**

**a) Transmitter**



**b) Receiver**

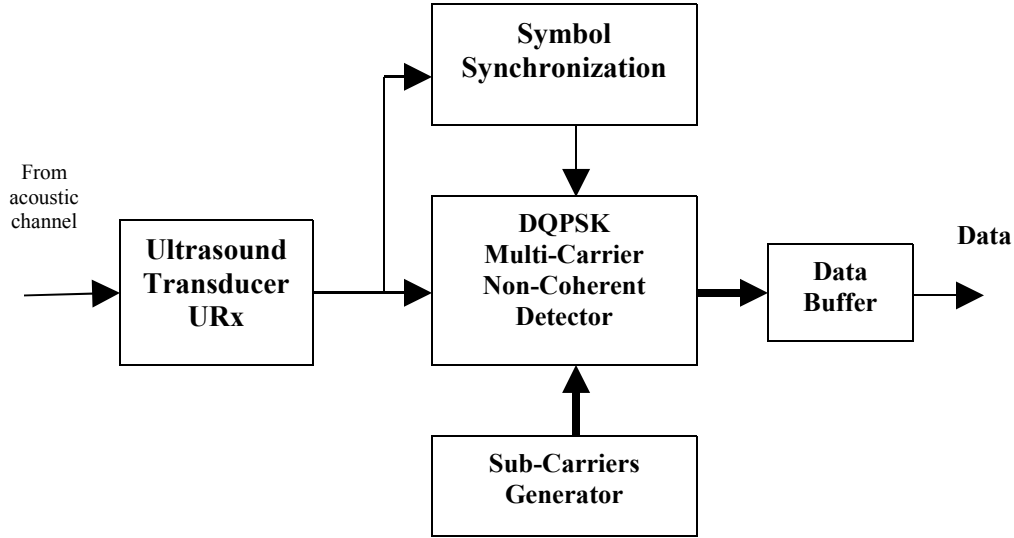


Fig.6 shows a high-level block diagram of the OFDM acoustic data transmission system, including an ultrasound transmitter and an ultrasound receiver. In the OFDM-DQPSK ultrasound transmitter (Fig.6a), binary data from a data source are first fed to a data buffer, which accumulates data for the current OFDM symbol. For example, in an OFDM-DQPSK acoustic system with 16 sub-carriers, the data buffer accumulates 32 bits (4 bytes), combined into 16 dibits (one dibit for each sub-carrier). Each dibit from the data buffer is differentially encoded, and the encoded dibit modulates the corresponding sub-carrier in the multiple DQPSK encoder/modulator. Then the modulated sub-carriers are summated in the summator. The summator outputs the signal to the transducer, which radiates the ultrasound waveform to the channel. In the OFDM-DQPSK ultrasound receiver (Fig.6b), the received ultrasound signal from the output of the URx transducer is fed to a symbol synchronization unit and a DQPSK multi-carrier detector. Using sub-carriers waveforms, generated the same manner as in the transmitter, the DQPSK detector, estimates sine and cosine functions of transmitted phase differences for all sub-carriers. Based on these estimations, the DQPSK detector provides multi-dibit decisions, transformed in the data buffer into a sequence of data bits. The non-coherent DQPSK detector operates for each sub-carrier according to the following algorithms. The first step – computation of correlation coefficients between the received signal  $R(t)$  and the quadrature references:

$$X_k = \sum_{n=1}^N R(n\Delta t) \sin[(k*2\pi/T_a)n\Delta t], \quad (2a)$$

$$Y_k = \sum_{n=1}^N R(n\Delta t) \cos[(k*2\pi/T_a)n\Delta t], \quad (2b)$$

where  $\Delta t$  is a sampling interval, and  $N$  is a number of signal samples within the active interval  $T_a$ ,  $k$  is a carrier number, and summation in (2) is provided for samples within  $T_a$ . The second step – computation of sine and cosine functions of the transmitted phase difference:

$$S_k = X_k X_{k^*} + Y_k Y_{k^*}, \quad (3a)$$

$$C_k = X_{k^*} Y_k - X_k Y_{k^*}, \quad (3b)$$

where  $X_{k^*}$  and  $Y_{k^*}$  – estimates (2a) and (2b) for the previous symbol interval. The third step – decision making as follows:

$$\text{If } |S_k| > |C_k| \text{ and } S_k > 0, \text{ then dibit} = 00, \quad (4a)$$

$$\text{If } |S_k| > |C_k| \text{ and } S_k < 0, \text{ then dibit} = 11, \quad (4b)$$

$$\text{If } |S_k| < |C_k| \text{ and } C_k > 0, \text{ then dibit} = 01, \quad (4c)$$

$$\text{If } |S_k| < |C_k| \text{ and } C_k < 0, \text{ then dibit} = 10. \quad (4d)$$

It should be noted that calculations (2), (3), and (4) are provided for all sub-carriers.

The symbol synchronization in the receiver can be realized by calculating correlation coefficients  $X_s$  and  $Y_s$  according to (2) for the skipped sub-carrier, for example, for the sub-carrier with number  $k=100$  in the OFDM signal in Fig.5a. It is clear that at perfect synchronization these values are equal to zero on average. So, the synchronization algorithm should find the active interval, which minimizes the length of vector  $(X_s, Y_s)$ . For this purpose, the synchronization block should calculate two vectors: vector  $(X_{s-}, Y_{s-})$  for an advanced active interval, and vector  $(X_{s+}, Y_{s+})$  for a delayed active interval. The squared lengths of these vectors are:

$$L_- = (X_{s-})^2 + (Y_{s-})^2, \quad (5a)$$

$$L_+ = (X_{s+})^2 + (Y_{s+})^2. \quad (5b)$$

A tracking algorithm should be realized based on the average  $L_-$  and  $L_+$ : if  $L_+ > L_-$ , the active interval should be shifted to left in time, and opposite, if  $L_+ < L_-$ , the active interval should be shifted to right in time.

It should be noted that the existing wireless OFDM technology includes Fast Fourier Transforms (FFT) and inverse FFT (IFFT) of signals in transmitters and receivers, based on comparatively complex computational procedures including arithmetic operations with complex numbers [6]. Besides, this technology usually includes coherent signal processing, which requires special pilot signals or complex carrier recovery with adaptive phase tracking. The considered above OFDM acoustic system is based on direct generation of the multi-carrier signal by means of summation of generated sub-carriers in the transmitter, as well as on direct correlation of the received signal and references in the receiver. Besides, optimal non-coherent processing does not require any pilot signal or the carrier recovery procedure because it is invariant to initial phases of the sub-carriers. All those features simplify signal processing in comparison with conventional OFDM wireless technology.

Stochastic MatLab simulation of the OFDM acoustic system with the DQPSK modulation according to block-diagram Fig.6 has been provided with a model of the AWGN channel. The OFDM signal included 16 orthogonal sub-carriers with different parameters indicated in Table 1. The DQPSK, based on Gray encoding (32 bits per OFDM symbol), and the

optimal non-coherent processing of DQPSK signals according to algorithms (2)-(4) were used in the simulation. The simulation shows that at the bit error rate BER=0.001, the OFDM-DQPSK system requires about 2-3 dB more radiated power than the FH-FSSK-DQPSK system (with orthogonal FH pulses) at the equal bit rates. It should be, however, noted that OFDM system has much more compact spectrum than the FH-FSSK system with orthogonal FH pulses, and OFDM signal can be radiated by single acoustic transducer.

The influence of acoustic transducer nonlinearity was also investigated by stochastic simulation of the OFDM-DQPSK system at different levels of transducer nonlinearity. The simulation shows that even a considerable transducer nonlinearity – deep clipping the transmitted signal – changes the acoustic system performance insignificantly comparing with the pure linear case. For example, at clipping level, corresponding to peak factor 1.7-1.9, the SNR lost does not exceed 0.8-1.0 dB. The reason of such negligible impact of nonlinearity is that majority of nonlinear products in this case are situated out of the OFDM signal bandwidth.

### **3. Modems for single-path acoustic intra-body channels**

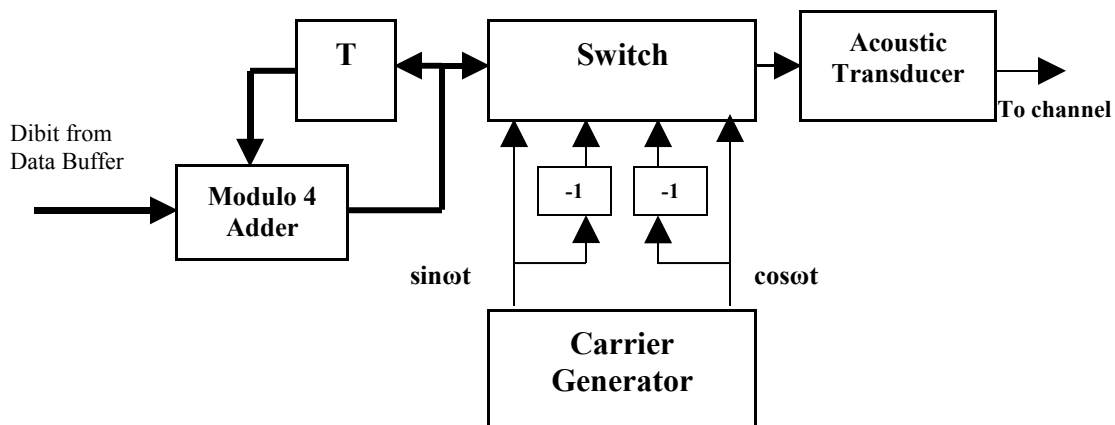
If echo-signals in the intra-body acoustic channel are considerably attenuated relatively the shortest path signal, then the data transmission system can use the simplest digital modulation scheme or even analog modulation scheme. Three reasonable options are described below.

#### **3.1. Single-carrier DQPSK modulation scheme.**

Utilization of the DQPSK modulation is one of the most preferable solutions for the single-path acoustic channel. First, it is comparatively simple in implementation. Second, it provides high frequency efficiency and noise robustness. Third, it allows the system to use non-coherent signal processing without any phase tracking in the receiving site [11] – it is a very important advantage for data transmission from a moving capsule in the intra-body acoustic channel.

**Fig.7 Block–diagram of the DQPSK acoustic system**

#### **a) Transmitter**



A scheme of an acoustic system based on non-coherent processing of DQPSK signals are shown in Fig.7. In the acoustic transmitter (Fig.7a), the transmitted dibit (00, 01, 10, or 11) from the data buffer is modulo 4 summated with a dibit, transmitted within the previous symbol interval and saved by delay element T, where T is the symbol duration. This DQPSK encoding is illustrated by Table 2:

**Table 2. Differential QPSK Encoding (Gray Code)**

Decimal presentation of the transmitted Dibit	Transmitted Dibit	Transmitted Phase difference $\Delta\Phi$	$\cos\Delta\Phi$	$\sin\Delta\Phi$
0	00	0	1	0
1	01	$\pi/2$	0	1
2	10	$3\pi/2$	0	-1
3	11	$\pi$	-1	0

The output of the modulo 4 adder controls a switch such a way that the switch outputs one of four carrier variants  $\pm\sin\omega t$ ,  $\pm\cos\omega t$ , generated by the carrier generator and two invertors. It should be noted that all DQPSK encoding operations - modulo 4 summation, and switch controlling - are performed one time per the DQPSK symbol; then, during the DQPSK symbol interval, the chosen carrier variant is transmitted without any changes. It should be also noted that the DQPSK transmitter may be digitally implemented based on a digital table of the carrier samples. In this case the carrier variants  $\pm\sin\omega t$ ,  $\pm\cos\omega t$  are generated by means of reading the table, which stores samples of functions  $\pm\sin\omega t$ ,  $\pm\cos\omega t$  in digital form. The table contains at least two columns ( $\sin\omega t$  and  $\cos\omega t$ ), and several rows (depending on sampling rate), representing at least 1/4 period of the carrier. The switch chooses one of columns with sign plus or minus depending on the output of the DQPSK encoder.

**b) Receiver**

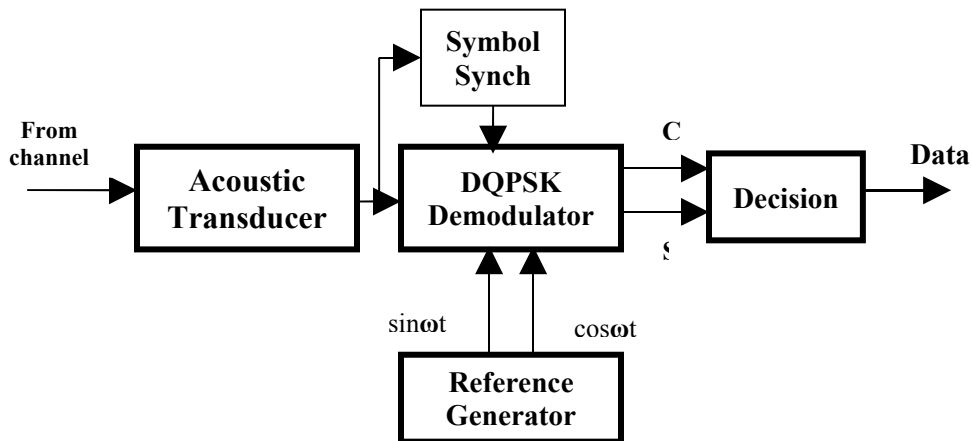
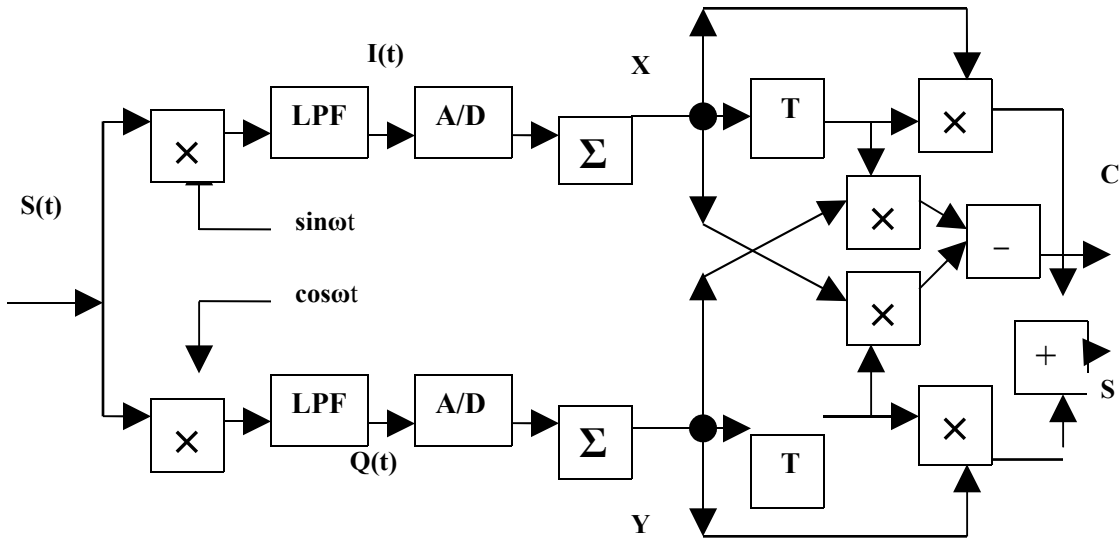


**Fig. 8 Scheme of the Optimal Noncoherent DQPSK Demodulator Based on Quadrature I/Q transforms**



In the acoustic receiver (Fig.7b), a local reference generator, generating the carrier signal with an arbitrary initial phase, provides quadrature references to a DQPSK demodulator. The scheme of the analog/digital non-coherent DQPSK demodulator is depicted in Fig.8. The front-end of the demodulator, including multipliers and low-pass filters (LPF), provides conventional transformation of the received signal into quadrature envelopes  $I(t)$  and  $Q(t)$ . Analog-to-digital converters and adder-accumulators  $\Sigma$  carry out digital integrating the convolution of the received signal and the reference according algorithm (2). The remaining part of the scheme in Fig.8 provides calculation of sine and cosine functions of the received phase difference according to algorithm (3). Finally, the scheme outputs signals to the decision block in Fig.7b, which provides bit decision according to algorithm (4).

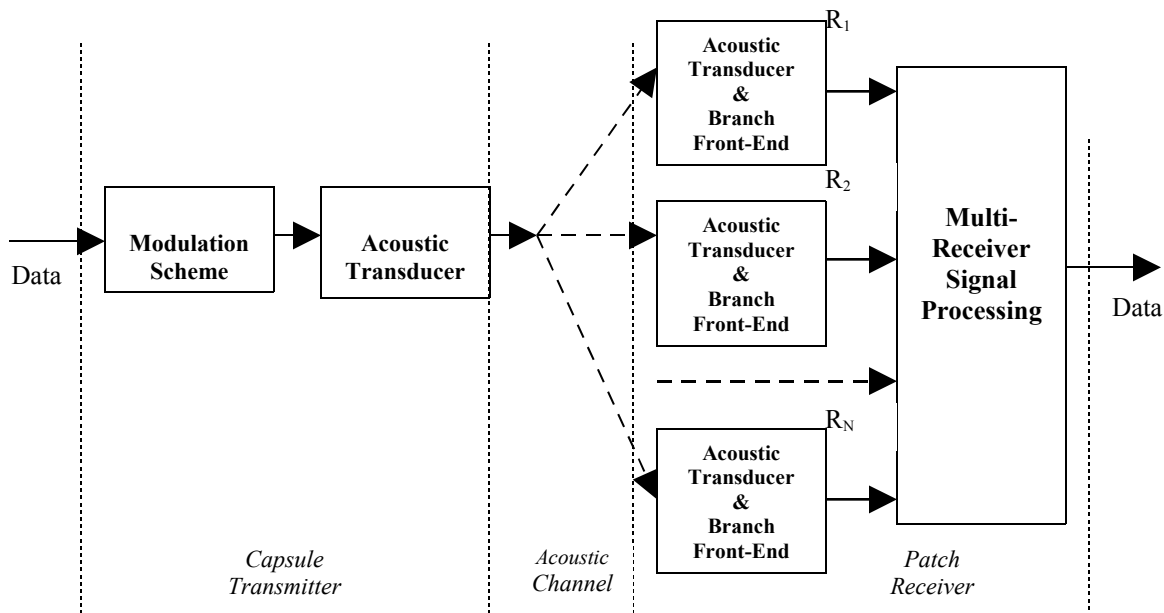
Theoretically [11] the considered non-coherent DQPSK modulation scheme provides the bit error rate  $BER=0.001$  at  $SNR=12.2$  dB at the input of the receiver. It loses 1.8 dB to the coherent DQPSK scheme and 2.3 dB to ideal coherent QPSK scheme. However, it should be noted that the coherent DQPSK and QPSK receivers need comparatively complex carrier recovery schemes, and the coherent QPSK receiver additionally requires transmission of a pilot signal; so, in reality, the energy loss of the considered non-coherent DQPSK modulation scheme is less than indicated above.

The DQPSK modulation scheme was simulated in MatLab and implemented experimentally. A LabView based DQPSK system with data rate up to 1 Mbit/s provided performance close to the theoretical limit. Based on the LabView software and Innurvation ultrasound hardware, an experimental acoustic data transmission system with the DQPSK modulation scheme was tested. The system included actual acoustic transducers in frequency range about 2 MHz, and a water tank media, imitating property of the intra-body acoustic channel. This experimental system has provided data transmission with bit rate up to 500 kbit/s at  $BER<0.001$ ; data rate restriction was caused by the limited bandwidth of real acoustic transducers, which did not exceed 250 kHz.

### 3.2. Multi-receiver acoustic system

Multi-receiver processing of data signals is considered to be a part of Multiple-Input-Multiple-Output (MIMO) technology, which is at present one of the most promising approaches to data transmission system design [12]. Modern MIMO technology is comparatively new innovation, but from the historical prospective, MIMO is direct development of the well-known space (spatial) diversity technique, which has been used in radio systems with multipath propagation for many decades. The space diversity technique can be successfully used in the intra-body acoustic channel by means of multiple patch-receivers located outside a human body. Multi-receiver processing provides considerable signal-to-noise gain and allows the system to decrease radiated power in both multipath and single-path channels.

**Fig.9 General block-diagram of the multi-receiver acoustic system**



A general block-diagram of the multi-receiver acoustic system is shown in Fig. 9. The transmitting site, located in the capsule, includes as usual a modulation scheme and an acoustic transducer, radiating a modulated carrier. The multi-receiving site, located in patches on a human body, contains N receivers (receiver branches) and a block of multi-receiver signal processing. Each branch includes a receiving acoustic transducer and an electronic branch-front-end. Each branch-front-end, in its turn, provides acoustic-electronic interface and preliminary signal processing. The block of multi-receiver signal processing provides combined (integrated) processing of branch signals as well as the final decision. It should be noted that the block of multi-receiver signal processing may be physically combined with one of the patch-branch-receiver or located in some separate device. Besides, processing functions can be physically divided between the branch-receivers and the block of multi-receiver processing.

Let us consider the multi-receiver signal processing for DQPSK modulation scheme. Because intra-body acoustic channel has fast variations of signal parameters, it is reasonable to consider multi-receiver processing based on non-coherent quadrature summation of the branch signals. Skipping some intermediate transforms, it can be found that the decision unit should determine the maximum among the following values:

$$\mathbf{V}_1 = \sum_{n=1}^N \mathbf{v}_{1n}; \mathbf{v}_{1n} = X_{1n}X_{2n} + Y_{1n}Y_{2n}; \quad \mathbf{V}_3 = -\mathbf{V}_1 \quad (6a)$$

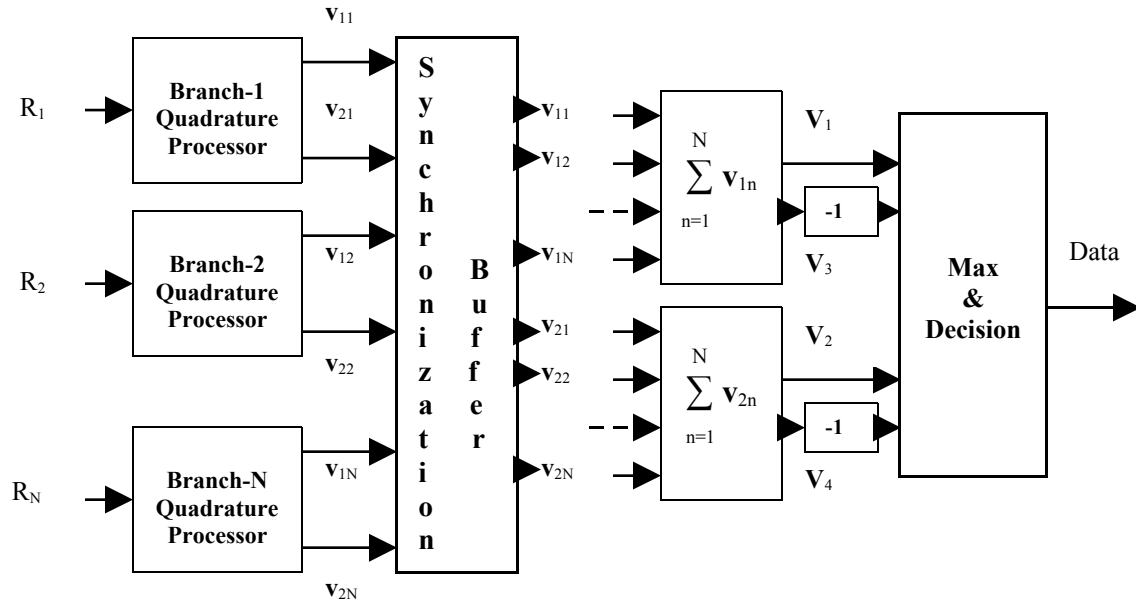
$$\mathbf{V}_2 = \sum_{n=1}^N \mathbf{v}_{2n}; \mathbf{v}_{2n} = X_{1n}Y_{2n} - Y_{1n}X_{2n}; \quad \mathbf{V}_4 = -\mathbf{V}_2 \quad (6b)$$

where  $n$  – receiving branch number,  $N$  – number of the receiving branches, and  $X_{1n}$ ,  $X_{2n}$ ,  $Y_{1n}$ , and  $Y_{2n}$  are determined as projections of the received signal  $R_n(t)$  of the  $n$ -th branch on the quadrature reference signals during the current and previous symbol intervals, namely:

$$X_{1n} = \int_0^T R_n(t) \sin \omega t \, dt; \quad X_{2n} = \int_T^{2T} R_n(t) \sin \omega t \, dt;$$

$$Y_{1n} = \int_0^T R_n(t) \cos \omega t \, dt; \quad Y_{2n} = \int_T^{2T} R_n(t) \cos \omega t \, dt.$$

**Fig.10 Block-diagram of the Multi-Receiver Signal Processing with quadrature accumulation of the DQPSK signals**



A block-diagram of the Multi-Receiver Signal Processing with quadrature accumulation of the DQPSK signals is depicted in Fig.10. The quadrature processor of the n-th branch calculates values  $v_{1n}$  and  $v_{2n}$  according to algorithms (6). It should be noted that the branch quadrature processors operate independently, and they have individual symbol synchronization units; the only common unit of the quadrature processors is a local carrier oscillator, providing reference signals for all quadrature processors. Independently calculated pairs  $(v_{1n}, v_{2n})$  for all  $n=1, 2, \dots, N$ , are then fed to the synchronization buffer, as it is indicated in Fig.10.

The synchronization buffer is one of the most important specific parts of this acoustic system, which conceptually separates acoustic multi-receiver processing from the conventional multi-receiver processing in radio systems. The function of this unit is to equalize time delays of different receiving branches at the input of accumulators. In contrast to radio channels, an acoustic channel has considerable signal delay difference between different branches. Assuming an ultrasound speed equal to 150000 cm/s, the delay difference  $\delta$  for distance difference  $\Delta D_{ij}$  cm between the capsule and the i-th and j-th branch-receivers can be estimated as  $\delta = \Delta D_{ij} / 150000$  s. If values  $\Delta D_{ij}$  change from zero through approximately 15 cm, then the delay difference will be  $0 < \delta < 10^{-4}$  s = 100 us. The last result shows that at symbol duration 10 us (bit rate 200 kbit/s for DQPSK), the delay difference can exceed 10 symbols, and at symbol duration 4 us (bit rate 500 kbit/s for DQPSK) the delay difference can exceed 25 symbols.

The output of the synchronization buffer contains the same sequence of vectors  $(v_{1n}, v_{2n})$  as the input of the synchronization buffer, however, a current set of vectors  $(v_{1n}, v_{2n})$  at the output of the buffer corresponds to the same symbols for all branches  $n=1, 2, \dots, N$ . Output buffer values  $v_{1n}$  and  $v_{2n}$  are separately combined at the inputs of 2 summators, which provide accumulation of 4 signal variants through all N branches according to algorithm (6). It should be noted that the summators actually accumulate only values  $v_{1n}$  and  $v_{2n}$  for calculating sums  $V_1$  and  $V_2$ ; sums  $V_3$  and  $V_4$  are calculated by changing the signs of sums  $V_1$  and  $V_2$ . Finally, the decision block selects the maximum from  $V_1, V_2, V_3$ , and  $V_4$  and determines the transmitted dibit. For example, dibit=00 if  $\max = V_1$ , dibit=01 if  $\max = V_2$ , dibit=11 if  $\max = V_3$ , and dibit=10 if  $\max = V_4$ .

Algorithms and schemes of the optimal quadrature accumulation of the branch signals, described above, are comparatively complex, mainly, because of the necessity to synchronize branch signals having considerable delays in acoustic channels (branch delay equalization). Simplification of the multi-receiver processing can be achieved by processing only one of branch signals having maximum SNR or maximum power of the received signal.

### 3.3. DSB/SSB analog acoustic system

The digital modulation schemes for multi-path and single-path acoustic channels considered above provide high performance in terms of SNR and frequency efficiency (bit/s/Hz). However, their bit rate depends significantly on the acoustic channel bandwidth. Conventionally, real acoustic transducers have bandwidth not more than 25% of their central frequency, i.e. 250-500 kHz in frequency area 1-2 MHz. Taking into account that it is difficult to realize more than 2 bit/s/Hz frequency efficiency at restricted computation resources, we can estimate data rate potential as 0.5-1.0 Mbit/s for acoustic channels in the 1-2 MHz frequency area. Sometimes image transmission from the capsule inside a body requires a higher bit rate, and digital modulation schemes cannot meet these requirements unless efficient image compression and/or data buffering is used in the capsule. In those cases, analog modulation schemes can provide an alternative solution.

Selection of an analog modulation scheme for the intra-body acoustic channel should be based on both its power and frequency efficiency in terms of the SNR gain and the analog signal bandwidth.

**Fig.11 Power Efficiency of the Analog Modulation Schemes**

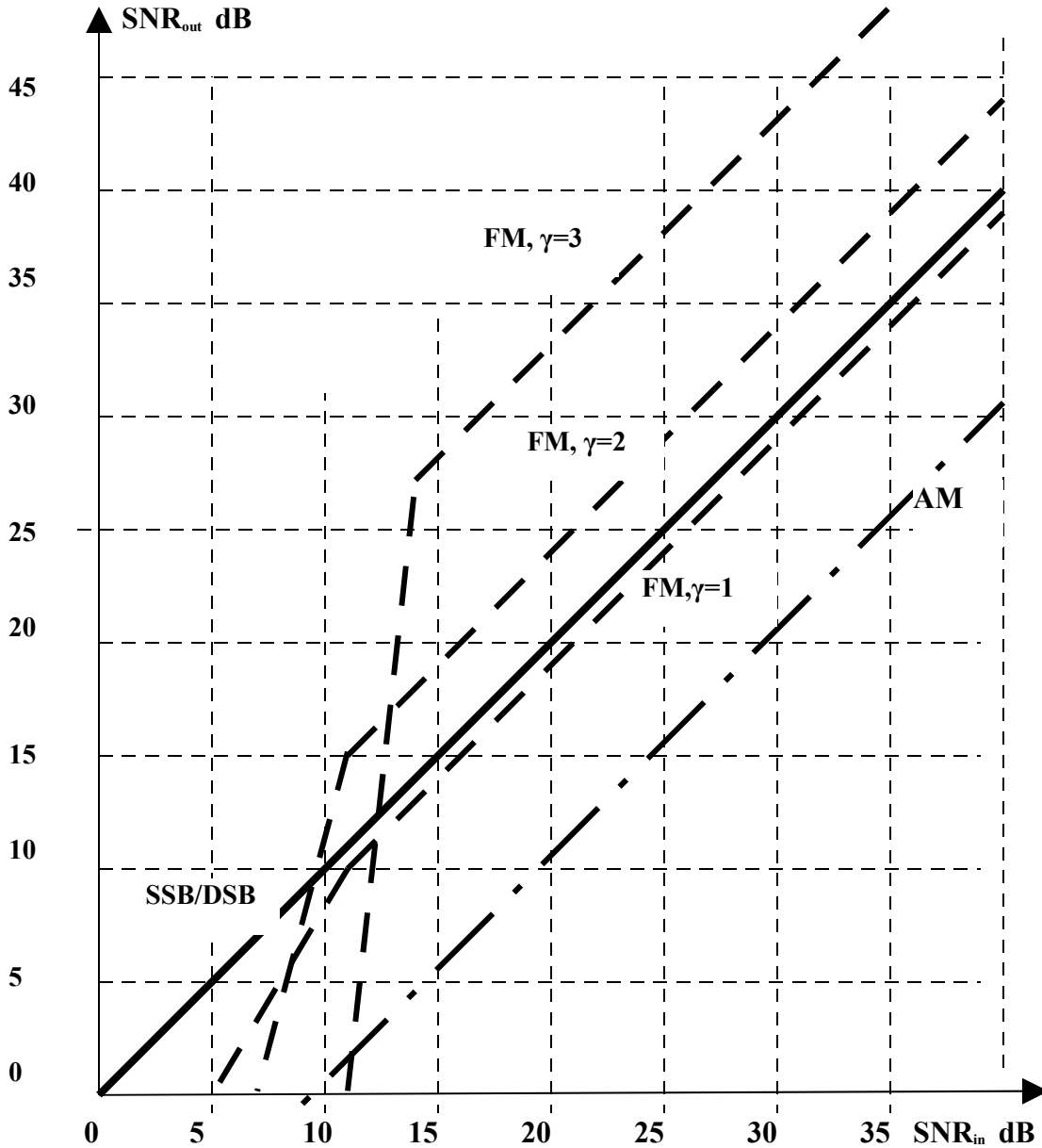
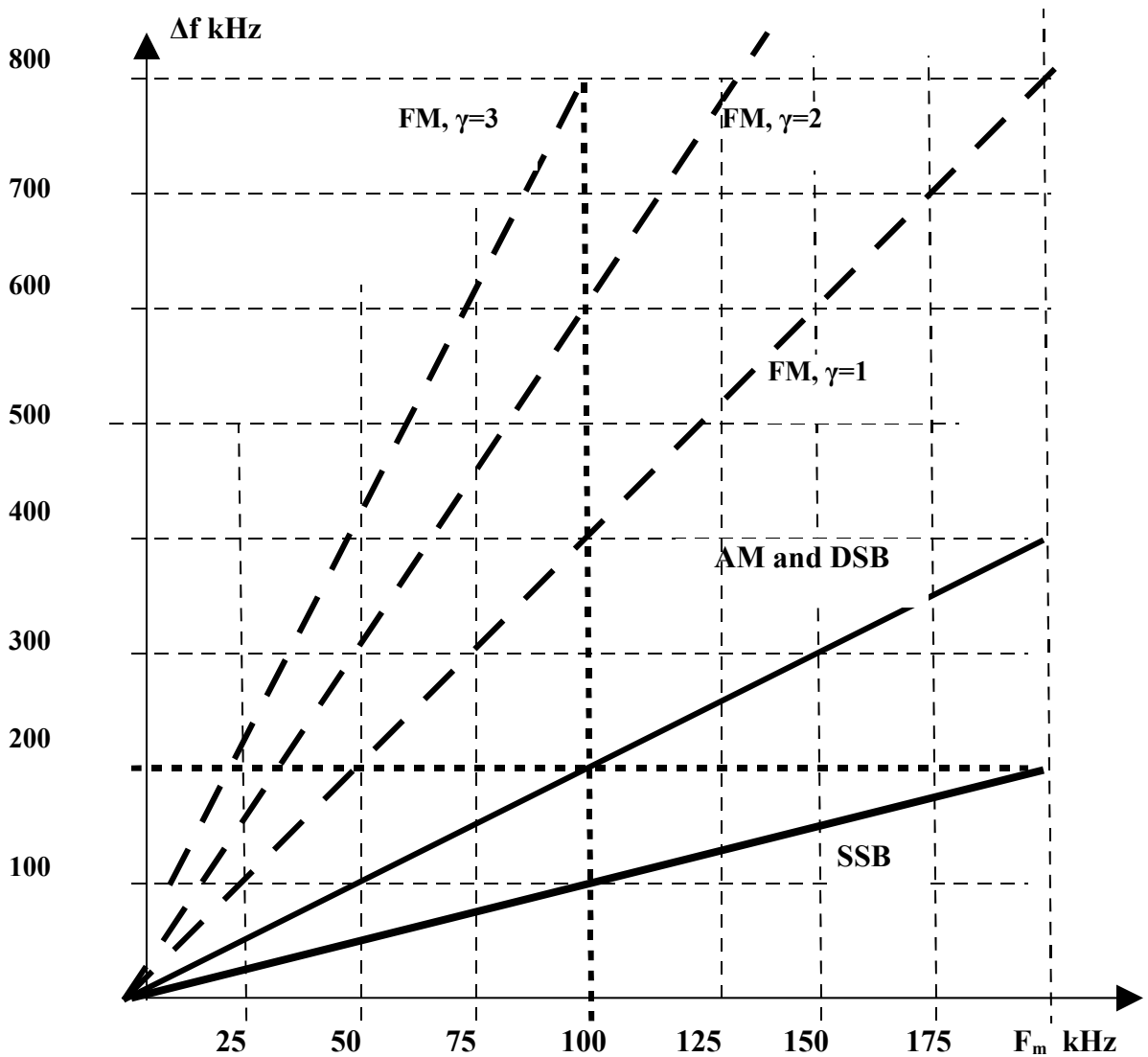


Fig. 11 provides a comparison of SNR gains for different analog modulation schemes: Amplitude Modulation (AM), Frequency Modulation (FM), Single Side-Band Modulation (SSB), and Double Side-Band Modulation (DSB), based on several literature sources [13,14]. The figure depicts the SNR<sub>out</sub> – the SNR at the output of the receiver, as a function of the SNR<sub>in</sub> – the SNR at the input of the receiver, for AM (dot-and-dash curve), FM (dash curves), SSB and DSB (solid curve) modulation schemes.

The AM system has minimum SNR gain  $G = \text{SNR}_{\text{out}}/\text{SNR}_{\text{in}} < 1$ . The curves for the FM system are calculated for message peak-factor  $p = P_{\text{max}}/P_{\text{average}} = 3$  and the FM indexes  $\gamma = \Delta f/F_m = 1, 2, 3$ , where  $\Delta f$  is the FM signal bandwidth in the acoustic channel, and  $F_m$  is the message bandwidth. The FM system has considerable SNR gain at  $\gamma > 1$  and  $\text{SNR}_{\text{in}} > 12$  dB; in the area  $\text{SNR}_{\text{in}} < 12$  dB, the FM SNR gain goes sharply down – the FM threshold effect [14].

As one can see from Fig.11, the SSB and DSB have SNR gain  $G = \text{SNR}_{\text{out}}/\text{SNR}_{\text{in}} = 1$ , which is approximately the same SNR gain as the FM SNR gain at  $\gamma = 1$  in the area  $\text{SNR}_{\text{in}} > 12$  dB. The FM with  $\gamma = 2$  has about 4 dB more SNR<sub>out</sub>, than the SSB/DSB, in the area  $\text{SNR}_{\text{in}} > 12$  dB; the FM with  $\gamma = 3$  has about 13 dB more SNR<sub>out</sub>, than the SSB/DSB, in the area  $\text{SNR}_{\text{in}} > 14$  dB.

**Fig.12 Frequency Efficiency of Analog Modulation Schemes**

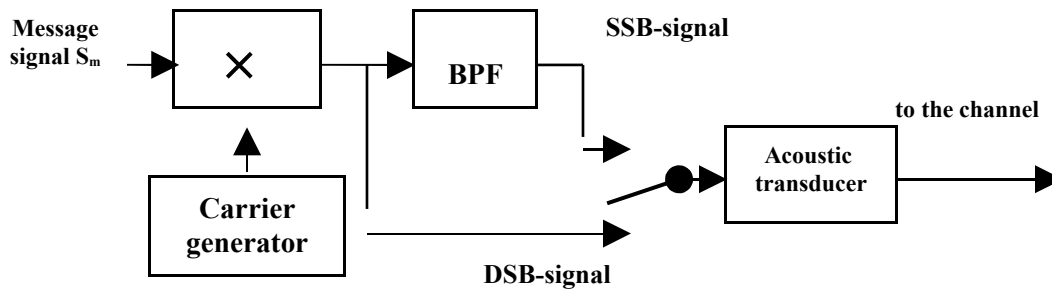


The comparison of SSB/DSB and FM modulation schemes should include frequency efficiency of these schemes, namely, the necessary channel bandwidth  $\Delta f$  as a function of the message bandwidth  $F_m$ . Fig. 12 illustrates this function for SSB, AM, DSB, and FM with FM indexes  $\gamma=1, 2, 3$ . As one can see, at the message bandwidth  $F_m=100$  kHz, SSB occupies  $\Delta f=100$  kHz, AM and DSB occupies  $\Delta f=200$  kHz, and FM occupies  $\Delta f=400$  kHz at  $\gamma=1$ ,  $\Delta f=600$  kHz at  $\gamma=2$ ,  $\Delta f=800$  kHz at  $\gamma=3$ .

So, comparing power and frequency efficiency of different analog modulation schemes shows that only SSB and DSB modulation schemes can meet the strong requirements of the intra-body image transmission system – minimization of the radiated power at the given image bandwidth and restricted bandwidth of the acoustic devices.

The modulation procedure in the SSB and DSB modulation schemes consists in frequency translation of the original analog message signal into the area of higher frequencies. That is why the SSB/DSB is sometimes referred to as frequency heterodyning. Both SSB and DSB are based on carrier suppression, therefore the SSB and DSB transmitters do not waste power for transmitting the carrier signal. On the other hand, the channel bandwidth necessary and sufficient for message transmission by means of the SSB is exactly equal to the message bandwidth, and the DSB needs double message bandwidth.

**Fig.13 Scheme of the acoustic DSB/SSB transmitter**



The simplest SSB/DSB acoustic transmitter (Fig.13) includes a carrier generator, a multiplier (mixer), a band-pass filter (BPF), and an acoustic transducer radiating either SSB or DSB signal. The message signal  $S_m(t)$  is first multiplied with the carrier signal  $S_c(t)=\cos 2\pi f_0 t$ , generated by the carrier generator. The output of the multiplier is the double sideband signal with the suppressed carrier (DSB-signal), which equal to

$$S_{DSB}(t) = S_m(t)\cos 2\pi f_0 t. \quad (7)$$

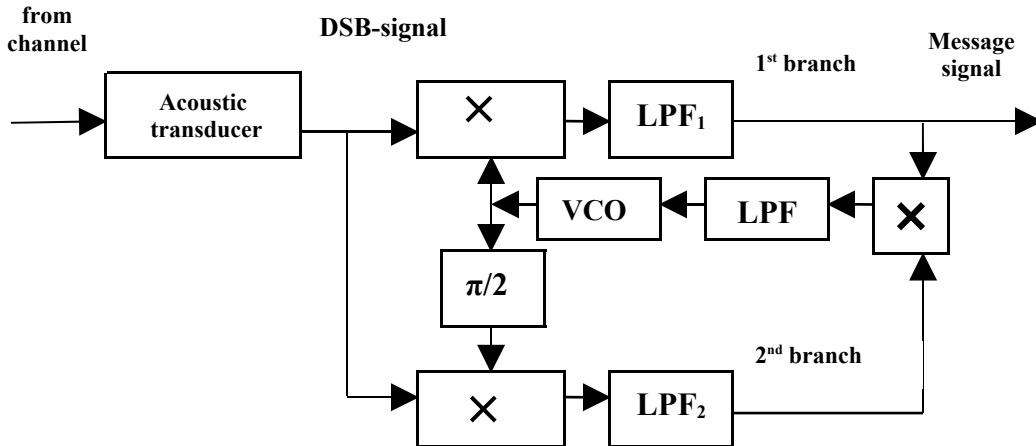
The BPF selects upper (or lower) side band of signal (7) and outputs the single side band signal with the suppressed carrier (SSB-signal), which can be described in time domain as follows:

$$S_{SSB}(t) = S_m(t)\cos 2\pi f_0 t - \mathbb{S}_m(t)\sin 2\pi f_0 t, \quad (8)$$

where  $\mathbb{S}_m(t)$  is the Hilbert transform of the message signal  $S_m(t)$ .

Usually, analog image signal is sensitive to phase distortions, therefore the coherent processing of the SSB/DSB signal should be utilized [14]. There are two main approaches to implementation of the SSB/DSB coherent processing: pilot and pilotless methods.

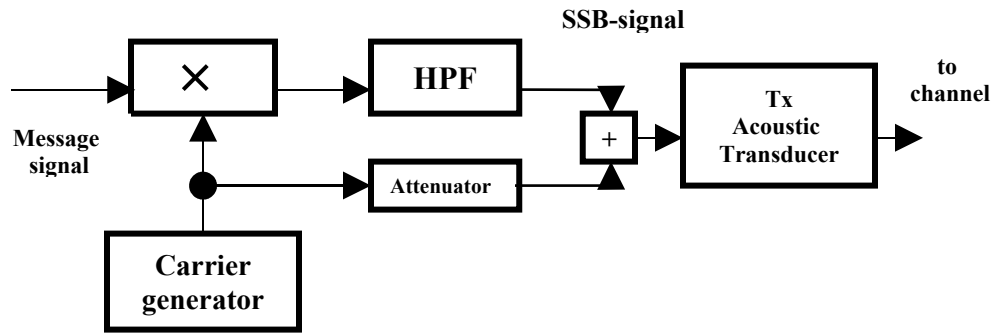
**Fig.14 Scheme of the acoustic DSB pilotless receiver**



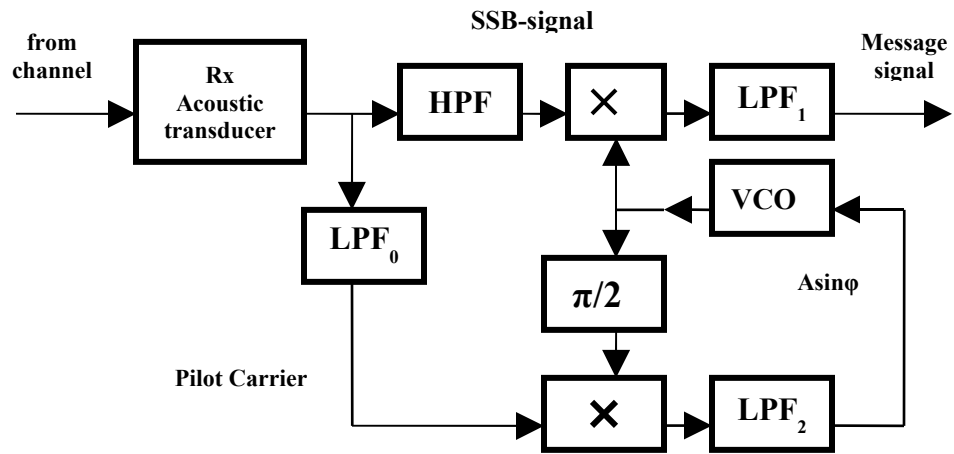
The DSB pilotless receiver (Fig.14) provides acoustic signal processing in two parallel quadrature branches including low-pass filters LPF<sub>1</sub> and LPF<sub>2</sub>, correspondingly. The coherent reference signal for both branches is generated by a voltage control oscillator (VCO), controlled through a feedback circuit by a phase discriminator, consisting of a multiplier and LPF<sub>0</sub>. This scheme of coherent carrier recovery is called Costas scheme [14].

**Fig.15 Scheme of the acoustic pilot system for image transmission by SSB modulation: a) – transmitter, b) – receiver.**

a)



b)



Schemes of the acoustic pilot system for image transmission by SSB modulation are shown in Fig.15. The SSB acoustic transmitter (Fig.15a) includes a carrier generator, a multiplier (mixer), a high-pass filter (HPF), and an attenuator. In this scheme, the attenuated carrier is added to the SSB signal in the summator. Combined signal is then radiated by the acoustic transducer. In the SSB acoustic receiver (Fig.15b), the received signal is divided into two parts - the SSB signal and the pilot carrier - by means of a high-pass filter (HPF) and low-pass filter ( $LPF_0$ ) with the same cut-off frequency for both filters. The SSB signal is then demodulated in the coherent demodulator, consisting of the local voltage control generator VCO, the multiplier, and low-pass filter  $LPF_1$ . The pilot carrier, in its turn, is compared with the local oscillation (shifted by  $\pi/2$ ), generated by VCO, in the phase discriminator, consisting of the multiplier and low-pass filter  $LPF_2$ . The output of the phase discriminator controls the VCO.

It should be noted that the SSB modem requires two times less acoustic channel bandwidth than the DSB modem for transmitting the same image. However, both the DSB transmitter and the DSB (pilotless) receiver are simpler than the corresponding parts of the SSB modem – it is considerable advantage of the DSB technique for the intra-body acoustic system.

## **Conclusion**

The transmission of image and telemetry data from a capsule inside a human body to outside receivers, based on modulation and encoding of ultrasound waves, is a new and promising approach to development of capsule endoscopy technology.

Both digital and analog modulation schemes can be used in the intra-body acoustic systems.

The most promising digital intra-body acoustic systems include the frequency hopping modulation scheme with combined frequency set shift keying and differential phase shift keying (FH-FSSK-DPSK), the multi-frequency modulation scheme with differential phase shift keying (OFDM-DPSK), the single carrier modulation scheme with differential quadrature (DQPSK), and the DQPSK modulation scheme with multi-receiver signal processing. The most efficient receivers (in terms of performance and implementation) for all type of the above modulation schemes are based on the optimal non-coherent signal processing. Digital acoustic intra-body systems can provide up to 0.5-1.0 Mbit/s data rate at BER=0.001 with real acoustic transducers in frequency range about 1-2 MHz.

The most promising analog intra-body acoustic systems include single side-band (SSB) and double side-band (DSB) modulation schemes with receivers based on the coherent signal processing. Analog acoustic intra-body systems can transmit image signals with the spectrum up to 125-250 kHz with real acoustic transducers in frequency range about 1-2 MHz.

## **References**

- [1] **Nakamura, T., and Terano, A.**, “Capsule endoscopy: past, present and future”, *Journal of Gastroenterology*, Vol. 43, # 2, 2008.
- [2] **Scapa, E. et al.**, “Initial experience of wireless-capsule endoscopy for evaluating occult gastrointestinal bleeding and suspected small bowel pathology”, *Journal of Gastroenterology*, Vol. 97, # 11, 2002.
- [3] **Iddan, G. et al.**, “Wireless capsule endoscopy,” *Nature*, Vol. 405, # 6785, 2000.
- [4] **Tae Song Kim et al.**, “Micro capsule endoscope for gastro intestinal tract”, 29th Annual International Conference of the IEEE EMBS, Lyon, France, 2007.

- [5] **Stojanovic, M.** (Editor) , “Underwater Wireless Communications ” (4 articles), IEEE Communications, Vol. 47, #1, 2009.
- [6] **Proakis, J.**, “Digital Communications”, McGraw-Hill, USA, 2001.
- [7] **Stojanovic, M.**, and **Preisig, J.**, “Underwater Acoustic Communication Channel: Propagation Models and Statistic Characterization”, IEEE Communications, Vol. 47, #1, 2009.
- [8] **Hashemi, H.**, "Impulse Response Modeling of Indoor Radio Propagation Channels", IEEE Journal on Selected Areas in Communications, Vol.11, #7, 1993.
- [9] **Simon, M. at al.**, “Digital Communications Techniques”, Prentice Hall, USA, 1995.
- [10] **Okunev, Y.**, “Theory of Phase-Difference Modulation”, Svyaz Press, Moscow, 1979.
- [11] **Okunev, Y.**, “Phase and Phase-Difference Modulation in Digital Communications”, Artech House, Boston-London, 1997.
- [12] **Jankiraman, M.**, “Space-Time Codes and MIMO Systems”, Artech House, Boston-London, 2004.
- [13] **Fink, L.** at al., “Theory of Signal Transmission”, Svyaz Press, Moscow, 1980.
- [14] **Haykin, S.**, “Communication Systems”, John Wiley & Sons, Inc., USA, 1994.